2017 International Conference on Rehabilitation Robotics (ICORR)
QEII Centre, London, UK, July 17-20, 2017.

Preliminary Results Toward a Naturally Controlled Multi-Synergistic Prosthetic Hand

Matteo Rossi[1,2], Cosimo Della Santina[2], Cristina Piazza[2],
Giorgio Grioli[1], Manuel Catalano[1], Antonio Bicchi[1,2]

***Abstract*— Robotic hands embedding human motor control principles in their mechanical design are getting increasing interest thanks to their simplicity and robustness, combined with good performance. Another key aspect of these hands is that humans can use them very effectively thanks to the similarity of their behavior with real hands. Nevertheless, controlling more than one degree of actuation remains a challenging task.**

In this paper, we take advantage of these characteristics in a multi-synergistic prosthesis. We propose an integrated setup composed of Pisa/IIT SoftHand 2 and a control strategy which simultaneously and proportionally maps the human hand movements to the robotic hand. The control technique is based on a combination of non-negative matrix factorization and linear regression algorithms. It also features a real-time continuous posture compensation of the electromyographic signals based on an IMU. The algorithm is tested on five healthy subjects through an experiment in a virtual environment. In a separate experiment, the efficacy of the posture compensation strategy is evaluated on five healthy subjects and, finally, the whole setup is successfully tested in performing realistic daily life activities.

I. INTRODUCTION

State of the art robotic and prosthetic hands are still far from bridging the gap with the human hand. The biomechanical complexity together with the advanced skills of the human sensory-motor system represent a big challenge for the development of new mechatronic solutions capable of the simultaneous, proportional and fluid movements and interactions of the human hand. Aiming to fill this gap, two main trends of research exist for robotic hand design. On one side, many hands are designed trying to match the many functions of human hands through complex design, including ingenious combinations of multiple motors and sensors. Noteworthy examples are [1][2]. These hands span a large range of movements and grasp shapes, but typically they have the drawback of being expensive and fragile. Furthermore, the problem of controlling them is in general very complex because of the large number of inputs that have to be managed. This makes them very hard to control for a human operator [3][4].

*This work was supported by the European Commission projects (Horizon 2020 research program) SOFTPRO (no. 688857) and by the European Research Council under the Advanced Grant SoftHands "A Theory of Soft Synergies for a New Generation of Artificial Hands" (no. ERC-291166)

[1]Department of Advanced Robotics, Istituto Italiano di Tecnologia, Genoa, Italy

[2]Centro di Ricerca "E. Piaggio", Universita di Pisa, Largo L. Lazzarino, 1, 56126 Pisa, Italy.

Correspond to: matteo.rossi at iit.it

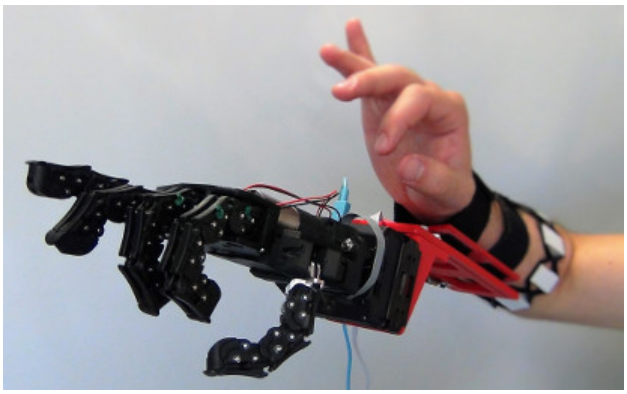

Fig. 1. Pisa/IIT SoftHand 2 controlled though MYO armband.

To overcome these limitations other hands were proposed following a minimalistic approach [5][6]. The main tools enabling their design are under-actuation [7], compliant mechanics [8], and a human-aware approach to system design [9]. These hands typically are characterized by a strongly simplified design and control interface, at the cost of a lower range of movements w.r.t. fully actuated hands. Among these hands, Pisa/IIT SoftHand+ was recently proposed [10]. SoftHand+ is a heavily under-actuated robotic hand, implementing two degrees of actuation, inspired by the most common human hand postures (namely postural hand synergies) as found in [11] and [12].

It is the authors' opinion that the reduced dimension of the actuation space, combined with the bio-inspired design, should make this class of under-actuated and soft hands a valuable candidate for applications where a human user is an active part of the planning and control loop, spanning from tele-operation, to prosthetics, to human grasp studies and rehabilitation robotics. The aim of this paper is to make a first step in the direction of developing a multi-synergistic prosthetic hand. We introduce a setup, composed of Pisa/IIT SoftHand 2 (Fig. 1), evolution of Pisa/IIT SoftHand+ [10], and a low cost myoelectric off-the-shelf input device, Myo Armband from Thalmic Labs [13]. In order to fully take advantage of the discussed characteristics of the robotic hand, we map proportionally and simultaneously the operator hand posture to the robotic system. We propose to achieve this goal through a controller which combines linear regression and non-negative matrix factorization (see subsection I-A for a detailed state of the art). Furthermore, we propose to use the arm posture acquired through the IMU provided by

the Myo Armband, to compensate for the artifacts found in electromyographic (EMG) signals due to limb position [14]. While other works have investigated the use of IMU data to increase the accuracy of classifiers [15] [16], to the best of our knowledge this is the first study that investigates the use of an IMU to directly compensate the EMG signals.

Experimental results are provided in order to demonstrate the effectiveness of the whole system, including a quantitative study of the algorithm in a real-time virtual environment with five subjects, and a qualitative study where an operator intuitively executes a set of realistic daily life activities.

A. State of the art in multi-DoF control

Myoelectric interfaces have been widely used to control assistive devices, and in particular upper-limb prostheses. However, myoelectric control of multiple degrees of freedom remains an open problem. The control strategy typically implemented in multi-DOF prostheses consists in the proportional control of a single DOF at a time with the possibility of switching between DOFs by a co-contraction signal. In the attempt to control multiple DOFs without the need for switching, a vast variety of classification-based approaches have been proposed [17]. Despite the good performance in classifying and control reached by these methods, they have strong limitations in terms of naturalness of control. Natural movements that involve two or more DOFs should be obtained by controlling the joints simultaneously and proportionally, but a classifier can only detect one function at time. By enriching the training set, it was shown that it is possible to achieve the simultaneous activation of multiple classes [18]. However, this approach can lead to a deterioration of classification accuracy and more complicated training sessions. For this reason, we focus our attention on a different class of control algorithms.

The use of regression techniques is an interesting alternative. These methods are applied to the simultaneous and proportional control of multiple DOFs, e.g. artificial neural networks (ANN) in [19], linear regression (LR) in [20] and non-negative matrix factorization (NMF) in [21]. Among the regression methods for EMG control, NMF presents several advantages. Besides being computationally efficient and requiring little user training, the non-negativity of the NMF approaches is in agreement with the fact that the firing rates of motor neurons can either increase or decrease but must always remain positive [22]. Also, it has been shown that the online performance of NMF is generally comparable or better than ANN and LR [23].

II. SETUP

Following the principle introduced in [10], we designed SoftHand 2 with a transmission system encompassing just one tendon, pulleys and two motors, each end of the actuation tendon is pulled by one of the two motors. Fig. 2(a) presents a sketch of SoftHand 2 , with the two motors underlined. SoftHand 2 inherits excellent grasp adaptability from Pisa/IIT SoftHand [24], which shares the first degree of actuation. Furthermore, thanks to the novel degree of actuation, Pisa/IIT SoftHand 2 can reach additional postures useful in daily life activities, such as grasping thin objects and pushing a button. Fig. 2(b) shows in the center the hand rest position and along the two axes the postures resulting from the application of the two degrees of actuation.

Fig. 3 presents the whole setup, composed of the robotic hand Pisa/IIT SoftHand 2 , the EMG system Myo armband, and a mechanical interface used to connect the robotic hand to the operator's arm. Myo armband, by Thalmic Labs, is a wearable device that features eight stainless steel EMG sensors and a nine-axis IMU, which consists of a three-axis accelerometer, a three-axis gyroscope, and a three-axis magnetometer. The EMG signals are sampled at a frequency of 200Hz, while the sampling frequency for the IMU data is 50Hz. The acquired data is streamed to a computer via Bluetooth communication. The choice of this device was driven by (i) the portability of the device and (ii) the on-board inclusion of an IMU, taking also in consideration its relatively low cost. The Myo also contains a vibro-tactile feedback device that the authors aim to integrate in the testing framework in the near future. In this work, the Myo armband is worn by each subject around the thickest part of the right forearm (approximately in the first proximal third of the forearm) where the electrodes can sense the activity of the main extrinsic hand muscles.

III. CONTROL ALGORITHM

A. Gesture choice

Many studies show that humans are able to correct content errors in the mapping between the desired hand position and the actual position of an avatar of their own hand. However a substantial amount of similarity eases the operator task of controlling the system [25], [26]. Following this idea, to test the Pisa/IIT SoftHand, the operator interface was a dedicated handle, as shown in Fig. 4. The user operates the handle lever with a motion that is somewhat similar to the first grasp synergy that the SoftHand implements as its degree of actuation. This interface was demonstrated to be very easy and intuitive, as shown e.g. in [27].

The problem of controlling the SoftHand 2 is more complex because of the device nature; in fact, in order to operate two synergies, two different commands have to be generated. Following the same idea, we decided to adopt a myoelectric interface that enables the user to operate the SoftHand 2 in a natural and intuitive way. While being an effective strategy for intuitive control, this control method also represents a step towards the conversion of the SoftHand 2 to a multi-synergistic hand prosthesis. Instead of opting for any set of independent hand movements that allowed the control of the 2 DOF hand, we selected the hand movements that most closely matched the movements performed by the SoftHand 2.

B. EMG Filtering and Posture Compensation

Normalized EMG signals $q_i, i \in \{1 \dots 8\}$ are acquired at $200Hz$ from the operator forearm, as depicted in Fig. 3 and

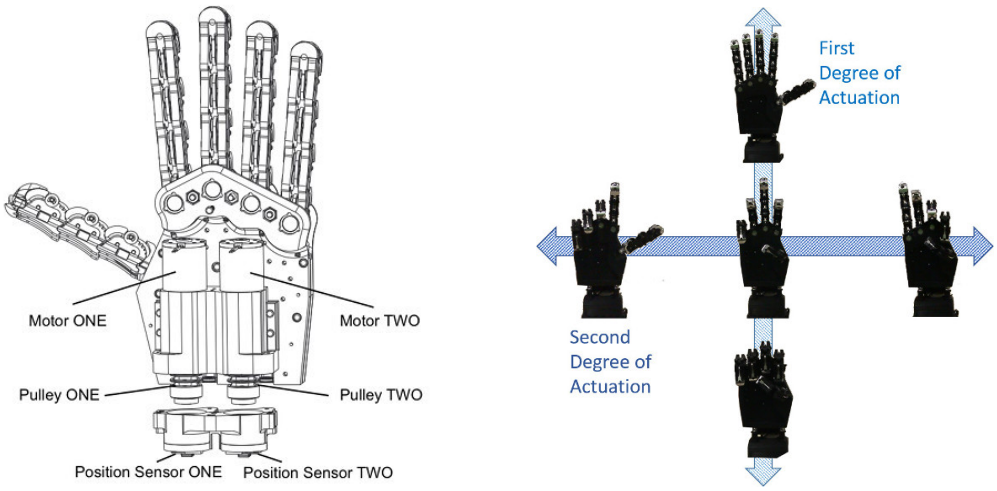

(a) Pisa/IIT SoftHand 2 (b) DoA

Fig. 2. (a) presents a sketch of Pisa/IIT SoftHand 2 with its two motors. (b) shows a representation of Pisa/IIT SoftHand 2 closures corresponding to the two degree of actuations (DoA). In the middle of the figure we report the hand rest position. The other four configurations are the extreme postures obtainable through one of the two degrees of actuations. All linear combinations of these two degrees are achievable by the hand.

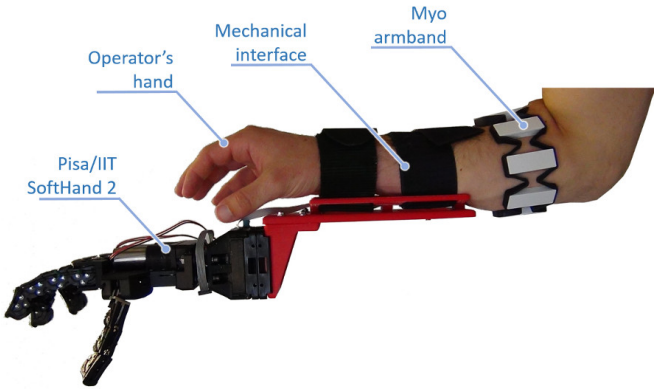

Fig. 3. Considered setup, composed of the Pisa/IIT SoftHand 2 , the mechanical interface to connect it to the user arm, and the Myo armband.

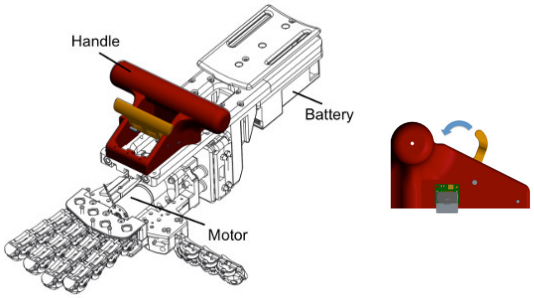

(a) (b)

Fig. 4. CAD model of Pisa/IIT SoftHand mounted on its handle. Note that the handle (a) is operated by squeezing a hand-lever (b), with a movement similar to that of the first synergy.

described in Sec. II. The mean absolute value (MAV) of the normalized signals is defined as

$$q_{f,i}(t) = \frac{1}{N} \sum_{k=t-N+1}^{t} |q_i(k)| \,, \tag{1}$$

where N is number of samples in the moving window and $q_{f,i}(t)$ is the MAV of q_i at time t. In this work, a moving window with $N = 40$ ($200ms$) is used.

In order to avoid undesired movement of the robotic hand when changing forearm posture with respect to gravity, a posture compensation technique was applied to the EMG signals. Note that along with the normalized EMG signals, Myo Armband also provides the orientation, in the form of quaternions, of the sensor frame $\mathscr{F}'$ with respect to an inertial reference frame $\mathscr{F}$. The angle γ between the Z axis of $\mathscr{F}'$ (forearm longitudinal axis, pointing proximally) and the Z axis of $\mathscr{F}$ (vertical axis with opposite direction with respect to gravity) is computed from the quaternion readings.

From the training data, an average μ_i of each filtered EMG signal $q_{f,i}$ is computed in 2 different postures: $\gamma = 0$ and $\gamma = \frac{\pi}{2}$, only for the values that correspond to a resting phase. Thus we propose here the following simple real-time compensation rule for the signals $q_{f,i}$

$$q_{c,i}(t) = \begin{cases} x_i(t), & \text{if} \quad x_i(t) \geq 0 \\ q_{f,i}(t), & \text{if} \quad x_i(t) < 0 \end{cases} \quad i = 1, \ldots, 8 \,, \tag{2}$$

where $x_i(t)$ is

$$x_i(t) = q_{f,i}(t) + (\cos\gamma(t) - 1)\frac{\mu_{i,\gamma=0}}{\mu_{i,\gamma=\frac{\pi}{2}}}. \tag{3}$$

Two examples of compensated signals are shown in Fig. 5. The compensated (in red) and non compensated (in blue) EMG signals from two different sensors are relative to the repetition of the same gesture in different orientations of the forearm. While the EMG activity detected by sensor 1 is not

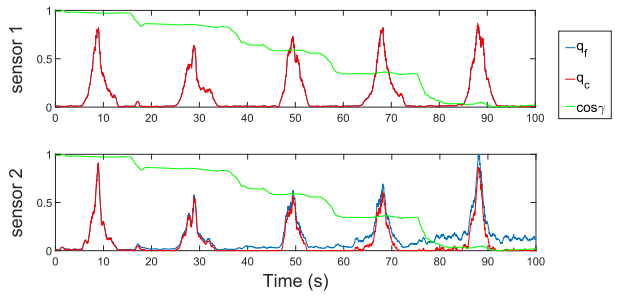

Fig. 5. Compensated (q_c) and non compensated (q_f) EMG signals acquired from two sensors during the repetition of the same hand gesture in different postures (increasing values of γ).

affected by the changes in posture, and thus the compensated and non compensated signals coincide, when $\cos\gamma$ (shown in green) is close to 0, the EMG activity detected by sensor 2 during rest phases may cause unwanted activations of the robotic hand, thus the compensation is desirable.

C. NMF

Non-negative matrix factorization (NMF) is a method for the factorization of a matrix $\mathbf{A} \in \mathbb{R}^{m\times T}$, into two matrices $\mathbf{S} \in \mathbb{R}^{m\times n}$ and $\mathbf{U} \in \mathbb{R}^{n\times T}$, with the requirement that the three matrices, $\mathbf{A}$, $\mathbf{S}$ and $\mathbf{U}$, can only have non-negative entries, i.e. $\mathbf{A} \approx \mathbf{SU}$.

The elements of $\mathbf{S}$ and $\mathbf{U}$ can be determined by optimizing an error function J between $\mathbf{A}$ and $\mathbf{SU}$. The most commonly used cost function J is

$$J = ||\mathbf{A} - \mathbf{SU}||_2, \tag{4}$$

where $||\cdot||_2$ denotes the 2-norm.
This optimization problem can be solved using a supervised approach [22] that exploits information on the intended movement during the training phase, allowing more robust and repeatable results. The matrix A is defined as

$$\mathbf{A} = \begin{bmatrix} a_1(0) & \cdots & a_1(T) \\ \vdots & \ddots & \vdots \\ a_m(0) & \cdots & a_m(T) \end{bmatrix}, \tag{5}$$

where the activation level for each movement, $a_k(t)$ with $k \in \{1 \ldots m\}$, is described by a value between 0 (relaxed state) and 1 (maximum intensity), and represents the activation intensity of movement k that is requested of the user during the training phase at the time instant t. Four different control movements ($m = 4$) are used, which correspond to two different directions for each degree of freedom.

The matrix $\mathbf{S}$ can be used to find an estimate of the activation intensity $\hat{\mathbf{a}}(t)$ by computing the product with the MAV of the filtered EMG signals (vector $\mathbf{u}(t)$)

$$\hat{\mathbf{a}}(t) = \begin{bmatrix} s_{1,1} & \cdots & s_{1,8} \\ \vdots & \ddots & \vdots \\ s_{4,1} & \cdots & s_{4,8} \end{bmatrix} \mathbf{u}(t) = \mathbf{Su}(t) \tag{6}$$

To obtain the two control signals needed, $y_1(t)$ and $y_2(t)$, it is sufficient to find, for each degree of freedom, the difference of the activation intensities that correspond to opposite directions

$$\mathbf{y}(t) = \begin{bmatrix} y_1(t) \\ y_2(t) \end{bmatrix} = \begin{bmatrix} 1 & 0 & -1 & 0 \\ 0 & 1 & 0 & -1 \end{bmatrix} \mathbf{Su}(t) \tag{7}$$

D. NMF + LR

During preliminary tests with NMF, we noticed that when a subject had to perform movements characterized by a high intensity of the muscular activity in the attempt of activating one DOF in a certain direction, the component related to the same DOF, but with opposite direction, was often activated as well. This results in a restriction of the control signals, as also shown by the experimental results in Sec. IV and V. In an attempt to solve this issue, we propose here to augment NMF algorithm adding a LR-based layer.

The NMF method previously described was compared to a cascade of NMF and LR. In particular, two regression models were trained for each DOF, for a total of four models. The models were trained on the output of the NMF algorithm

$$\hat{\mathbf{a}}'(t) = \mathbf{B}^{\mathbf{T}}\mathbf{Su}(t), \tag{8}$$

where $\hat{\mathbf{a}}'(t)$ is the vector of the estimated activation levels for the four movements at the instant t and $\mathbf{B} \in \mathbb{R}^{mxm}$ contains the weight vectors. Given a training-set composed of T time instances, the entries of $\mathbf{B}$ were found by solving the equation

$$\mathbf{B} = (\mathbf{SUU}^{\mathbf{T}}\mathbf{S}^{\mathbf{T}})^{-1}\mathbf{SUA}^{\mathbf{T}}. \tag{9}$$

Once the elements of $\mathbf{B}$ are found, the product $\mathbf{B}^{\mathbf{T}}\mathbf{S}$ can be calculated offline during the training phase and the new estimate $\hat{\mathbf{a}}'(t)$ can be computed in real-time with no additional computational cost with respect to $\hat{\mathbf{a}}(t)$.
Similar to the previous case, to obtain the two control signals needed, it is sufficient to find, for each degree of freedom, the difference of the activation intensities that correspond to opposite directions

$$\mathbf{y}(t) = \begin{bmatrix} y_1(t) \\ y_2(t) \end{bmatrix} = \begin{bmatrix} 1 & 0 & -1 & 0 \\ 0 & 1 & 0 & -1 \end{bmatrix} \mathbf{B}^{\mathbf{T}}\mathbf{Su}(t). \tag{10}$$

IV. EXPERIMENTS

To test the effectiveness of the whole system, three different on-line tests were performed by healthy naive subjects. First, a target acquisition experiment was performed to assess and compare NMF and the here proposed NMF+LR. Then, a balance experiment was executed, to evaluate the effectiveness of the proposed posture compensation. Finally, one of the subjects performed additional qualitative tests composed of a set of daily activity tasks. Each subject provided written informed consent.

All tests were designed to evaluate performance on-line. Indeed many studies in the literature show how the off-line performance of a myoelectric control algorithm has little predictive value with respect to its on-line control performance [19] [23].

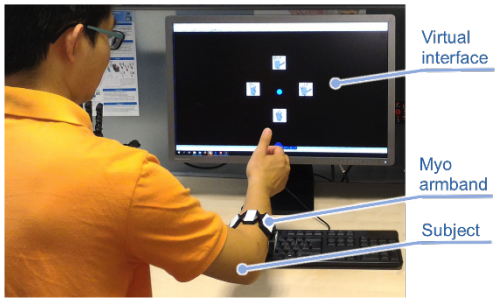

Fig. 6. Setup used for target acquisition experiment. The virtual interface consists of four hand posture representation and a target (represented by a blue sphere) that moves randomly between the hand postures. Each subject was asked to follow the moving target. During the experiment, the subject wore a MYO armband.

A. Target Acquisition Experiment

To compare NMF and NMF+LR within the proposed setup, five subjects performed a target acquisition task in a virtual environment. Both algorithms were trained on the same training-set, consisting of 60 seconds of EMG acquisition during which each subject had to replicate the four hand postures shown in Fig. 2(b) with increasing muscle activation. During the task, the control signals extracted by the EMGs were used to control the position of a cursor (blue sphere) on the screen (see Fig. 6). Prior to the test, it was verified that the subjects were able to perform the main movements at full range with and without compensation (positions $(0,1)$, $(1,0)$, $(0,-1)$ and $(-1,0)$ on the screen). To complete the test, the subjects were asked to reach a fixed target (red sphere) as quickly as possible, and to keep the cursor on it until it disappeared. This happened after 500 consecutive milliseconds in which the two spheres overlapped. If the target was not acquired during the first $10s$, the attempt was regarded as a failure and the red sphere disappeared. After a target disappeared, another target appeared after $4s$ of rest. Target were presented at a distance of 50%, 75% and 100% of the total range, with angles of $0, \frac{\pi}{8}, \frac{2\pi}{8}, \ldots, \frac{15\pi}{8}$ with respect to the vertical (see Fig. 7). The targets were presented in random order to each subject.

To assess the performance of the subjects, four outcome measures as described in [19] were used: *acquisition rate*, *path efficiency*, *completion time* and *overshoot*.

B. Balance Experiment

A balance experiment was also performed by five healthy subjects to assess the performance of the EMG compensation strategy. The whole setup was worn on the subjects' right forearm using the wearable mechanical interface of Fig. 3. The subjects were asked to perform the training procedure for the control algorithm two times, keeping the forearm horizontal ($\gamma = \frac{\pi}{2}$) and vertical ($\gamma = 0$) respectively. The parameters for the compensation were then extracted as described in III-B.

Using the virtual environment described in the previous experiment, the control signals extracted from the EMGs were mapped to the position of the cursor. The control range was mapped to a circular area of radius 1 on the screen (Fig. 6 and Fig. 7). Prior to the test, it was verified that the subjects were able to perform the main movements at full range with and without compensation , keeping the forearm in three different orientations ($\gamma \approx 0$, $\gamma \approx \frac{\pi}{4}$ and $\gamma \approx \frac{\pi}{2}$).

The test consisted in keeping the cursor in the origin (relaxed state) for 5 consecutive seconds, with the forearm respectively in $\gamma \approx 0$, $\gamma \approx \frac{\pi}{4}$ and $\gamma \approx \frac{\pi}{2}$ conditions, and without the aid of visual feedback. As performance metric we considered the average distance of the cursor from the origin.

TABLE I

RESULTS OF THE TARGET ACQUISITION EXPERIMENT AVERAGED ACROSS ALL SUBJECTS.

	NMF	NMF + LR	p-Value
Acquisition rate (%)	77.08 ± 0.13	92.08 ± 5.39	0.02
Path efficiency (%)	43.16 ± 6.54	44.63 ± 5.99	> 0.1
Completion time (s)	2.68 ± 0.30	2.17 ± 0.10	0.04
Overshoot	0.55 ± 0.28	0.61 ± 0.10	> 0.1

C. Qualitative Test

One subject participated in the qualitative test. During the test, the subject was presented with some realistic tasks and was let free to accomplish them in the way he considered the most efficient. The tasks focused on activities of daily living and bi-manual coordination. They included grasping a banknote, switching the lights off, firmly grasping a hammer, placing an egg in an egg carton, grasping an apple and extracting a credit card from a wallet.

V. RESULTS & DISCUSSION

A. Target Acquisition Experiment

Table I summarizes the performance of the control schemes during the target acquisition task, for the various performance metrics, averaged across all users. The NMF+LR method outperformed the NMF method in terms of *acquisition rate* (with a p-value of $p = 0.02$), and produced significantly lower *completion time* ($p = 0.04$). No significant difference was found in terms of *path efficiency*, and NMF performed slightly better in terms of *overshoot* with respect to NMF+LR, although the difference was not statistically significant ($p > 0.1$).

Fig. 7 illustrates the average *acquisition rate* for each target. Each dot represents a target. Its color encodes the number of times that it was acquired, from 0 (black) to 5 (white). Subjects were able to acquire all the targets that were at a distance of 50% of the total range, for both NMF and NMF+LR. Instead with targets at a distance of 75% and 100% of the total range, the here proposed NMF+LR method performs much better.

These results show a reduction of *acquisition rate* obtained with the NMF algorithm w.r.t. some other results presented in the literature (as e.g. [22] [28] [29]). This is probably due to the different hardware employed for EMG acquisition, which is less precise w.r.t. the ones used in the previously referred

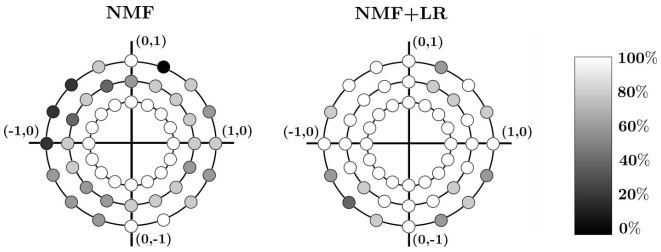

Fig. 7. Graphical representation of the average *acquisition rate* for each target. Each dot represents a target and its color represents the number of times that the target was acquired, from 0% of the times (black) to 100% of the times (white).

TABLE II

RESULTS OF THE BALANCE EXPERIMENT AVERAGED ACROSS ALL SUBJECTS.

	Compensation OFF	Compensation ON	p-Value
case $\gamma \approx 0$	0.06 ± 0.03	0.05 ± 0.03	> 0.1
case $\gamma \approx \frac{\pi}{4}$	0.15 ± 0.05	0.05 ± 0.02	0.03
case $\gamma \approx \frac{\pi}{2}$	0.25 ± 0.05	0.03 ± 0.02	0.01

papers. This, however, does not affect the significance of these results, since both algorithms are tested here on such a setup.

B. Balance Experiment

The results of the balance experiment are shown in Table II. When the forearm was kept in a vertical position ($\gamma \approx 0$), the average distance between the cursor and the origin was kept low ($< 10\%$ of the total range) for both the compensated and the non-compensated conditions. No statistical difference between the two conditions was found in this case ($p > 0.1$). In the other conditions, i.e. when the forearm was kept respectively at a 45° angle ($\gamma \approx \frac{\pi}{4}$) and 0° angle ($\gamma \approx \frac{\pi}{2}$) from the horizontal plane, the non-compensated condition resulted in higher distances of the cursor from the origin (respectively $> 10\%$ and $> 20\%$ of the total range), while the compensated condition resulted in low distances ($< 10\%$ of the total range). Thus in all the considered cases the proposed compensation algorithm outperforms or is at least equivalent w.r.t. the non-compensated condition.

C. Daily Life Activities

Fig. 8 shows the ability of the proposed algorithm in mapping the operator hand posture to the robotic hand, for all four postures of Fig. 2(b). Fig. 9 and 10 show the execution of some of the tasks during the qualitative test. In particular, Fig. 9 illustrates two different closures that can be used to accomplish the same task (grasping a banknote) in different ways. As shown in Fig.10, during the test the subject was able to successfully switch buttons (a), grasp heavy objects (b), manipulate fragile objects (c) and grasp thin objects (d). Finally Fig. 11 shows photo-sequences of complex daily activities, which also involve bi-manual operations. Additional examples can be found on the video attachment, also available at [30].

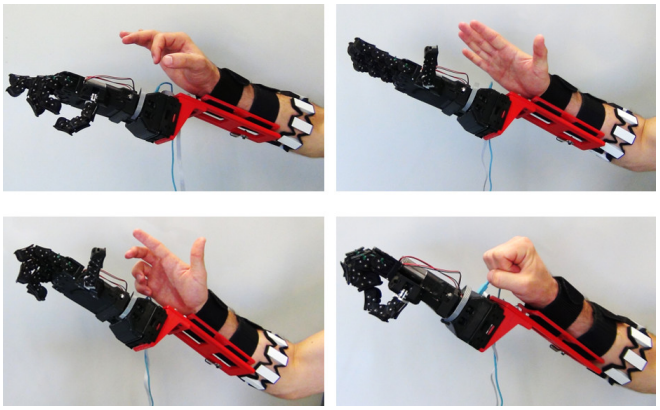

Fig. 8. The proposed control policy successfully maps on Pisa/IIT SoftHand 2 the subject hand postures correspondent to the two DoA, achieving the goal discussed in sec. III-A.

Fig. 9. An example of power and pinch grasp of a banknote. The similarity between the posture of an operator's hand and the Pisa/IIT SoftHand 2 highlights the effectiveness and the simplicity of this control strategy.

VI. CONCLUSIONS

In this paper, the online performance of two control algorithms based on NMF and NMF+LR techniques, were compared in order to choose a suitable candidate for the control of the SoftHand 2. A strategy to compensate for the influence of static postures on EMG signals was also implemented. The results of the balance experiment showed that when the compensation strategy was active, it allowed the subjects to maintain a *rest* command to the robotic hand while keeping their hand at rest in different positions. On the other hand, when the compensation strategy was not active, on average, unwanted commands as big as 25% of the total control range were generated by the subjects while keeping their hand at rest. Finally the whole setup was successfully tested by a healthy subject for the control of the SoftHand 2 in a realistic scenario to perform daily life activities. This

(a) (b) (c) (d)

Fig. 10. Some examples of grasps using different postures of the Pisa/IIT Softhand 2: switch buttons (a), grasp heavy objects (b), manipulate fragile objects (c) and pinch grasp of thin objects (d).

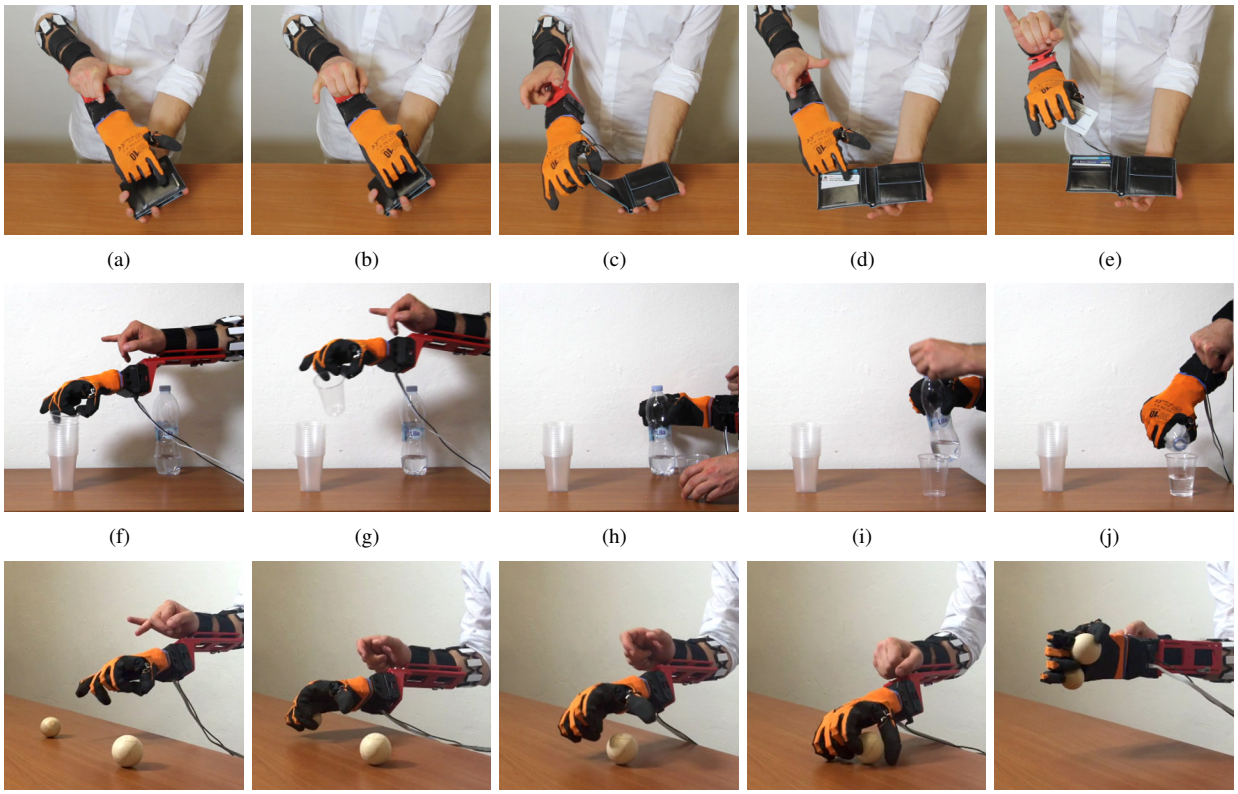

(a) (b) (c) (d) (e)

(f) (g) (h) (i) (j)

(k) (l) (m) (n) (o)

Fig. 11. Complex activities performed combining different postures of the hand: in (a-e) the subject opens a wallet and grasps a credit card, while in (f-j) he pours water into a glass, and in (k-o) a two phase grasp is performed on two distant objects.

new system will enable exploring the possibility of using the SoftHand 2 in prosthetics. Further work will be devoted in advancing the proposed setup both on hardware and control sides, with the long term goal of evolving Pisa/IIT SoftHand 2 into a multi-synergistic prosthetic device.

ACKNOWLEDGMENT

The authors would like to thank Alberto Brando, Andrea Di Basco, Alessandro Raugi and Fabio Bonomo for their really valuable support in the development of the hardware prototype and Gianluca Lentini, Ibrahim Kaoula and Francesco Amerotti for their help with the software development.

REFERENCES

[1] M. Grebenstein, A. Albu-Schäffer, T. Bahls, M. Chalon, O. Eiberger, W. Friedl, R. Gruber, S. Haddadin, U. Hagn, R. Haslinger *et al.*, "The dlr hand arm system," in *Robotics and Automation (ICRA), 2011 IEEE International Conference on*. IEEE, 2011, pp. 3175–3182.

[2] A. Kochan, "Shadow delivers first hand," *Industrial robot: an international journal*, vol. 32, no. 1, pp. 15–16, 2005.

[3] J. T. Belter, J. L. Segil, and B. SM, "Mechanical design and performance specifications of anthropomorphic prosthetic hands: a review," *Journal of rehabilitation research and development*, vol. 50, no. 5, p. 599, 2013.

[4] C. Piazza, C. Della Santina, M. Catalano, G. Grioli, M. Garabini, and A. Bicchi, "Softhand pro-d: Matching dynamic content of natural user commands with hand embodiment for enhanced prosthesis control," in *Robotics and Automation (ICRA), 2016 IEEE International Conference on*. IEEE, 2016, pp. 3516–3523.

[5] L. U. Odhner, L. P. Jentoft, M. R. Claffee, N. Corson, Y. Tenzer, R. R. Ma, M. Buehler, R. Kohout, R. D. Howe, and A. M. Dollar, "A compliant, underactuated hand for robust manipulation," *The International Journal of Robotics Research*, vol. 33, no. 5, pp. 736–752, 2014.

[6] R. Deimel and O. Brock, "A novel type of compliant and underactuated robotic hand for dexterous grasping," *The International Journal of Robotics Research*, p. 0278364915592961, 2015.

[7] L. Birglen, T. Laliberté, and C. M. Gosselin, *Underactuated robotic hands*. Springer, 2007, vol. 40.

[8] A. Albu-Schaffer, O. Eiberger, M. Grebenstein, S. Haddadin, C. Ott, T. Wimbock, S. Wolf, and G. Hirzinger, "Soft robotics," *IEEE Robotics & Automation Magazine*, vol. 15, no. 3, pp. 20–30, 2008.

[9] A. Bicchi, M. Gabiccini, and M. Santello, "Modelling natural and artificial hands with synergies," *Philosophical Transactions of the Royal Society B: Biological Sciences*, vol. 366, no. 1581, pp. 3153–3161, 2011.

[10] C. Della Santina, G. Grioli, M. Catalano, A. Brando, and A. Bicchi, "Dexterity augmentation on a synergistic hand: The pisa/iit softhand+," in *Humanoid Robots (Humanoids), 2015 IEEE-RAS 15th International Conference on*. IEEE, 2015, pp. 497–503.

[11] M. Santello, M. Flanders, and J. F. Soechting, "Postural hand synergies for tool use," *The Journal of Neuroscience*, vol. 18, no. 23, pp. 10 105–10 115, 1998.

[12] M. Gabiccini, G. Stillfried, H. Marino, and M. Bianchi, "A data-driven kinematic model of the human hand with soft-tissue artifact compensation mechanism for grasp synergy analysis," in *Intelligent Robots and Systems (IROS), 2013 IEEE/RSJ International Conference on*. IEEE, 2013, pp. 3738–3745.

[13] Myo Armband, "https://www.myo.com/."

[14] R. N. Khushaba, A. Al-Timemy, S. Kodagoda, and K. Nazarpour, "Combined influence of forearm orientation and muscular contraction on emg pattern recognition," *Expert Systems with Applications*, vol. 61, pp. 154–161, 2016.

[15] A. Fougner, E. Scheme, A. D. Chan, K. Englehart, and Ø. Stavdahl, "Resolving the limb position effect in myoelectric pattern recognition," *IEEE Transactions on Neural Systems and Rehabilitation Engineering*, vol. 19, no. 6, pp. 644–651, 2011.

[16] M. T. Wolf, C. Assad, M. T. Vernacchia, J. Fromm, and H. L. Jethani, "Gesture-based robot control with variable autonomy from the jpl biosleeve," in *Robotics and Automation (ICRA), 2013 IEEE International Conference on*. IEEE, 2013, pp. 1160–1165.

[17] M. A. Oskoei and H. Hu, "Myoelectric control systemsa survey," *Biomedical Signal Processing and Control*, vol. 2, no. 4, pp. 275–294, 2007.

[18] A. J. Young, L. H. Smith, E. J. Rouse, and L. J. Hargrove, "Classification of simultaneous movements using surface emg pattern recognition," *IEEE Transactions on Biomedical Engineering*, vol. 60, no. 5, pp. 1250–1258, 2013.

[19] A. Ameri, E. N. Kamavuako, E. J. Scheme, K. B. Englehart, and P. A. Parker, "Real-time, simultaneous myoelectric control using visual target-based training paradigm," *Biomedical Signal Processing and Control*, vol. 13, pp. 8–14, 2014.

[20] J. Hahne, F. Biessmann, N. Jiang, H. Rehbaum, D. Farina, F. Meinecke, K.-R. Müller, and L. Parra, "Linear and nonlinear regression techniques for simultaneous and proportional myoelectric control," *IEEE Transactions on Neural Systems and Rehabilitation Engineering*, vol. 22, no. 2, pp. 269–279, 2014.

[21] N. Jiang, K. B. Englehart, and P. A. Parker, "Extracting simultaneous and proportional neural control information for multiple-dof prostheses from the surface electromyographic signal," *IEEE Transactions on Biomedical Engineering*, vol. 56, no. 4, pp. 1070–1080, 2009.

[22] C. Choi and J. Kim, "Synergy matrices to estimate fluid wrist movements by surface electromyography," *Medical engineering & physics*, vol. 33, no. 8, pp. 916–923, 2011.

[23] N. Jiang, I. Vujaklija, H. Rehbaum, B. Graimann, and D. Farina, "Is accurate mapping of emg signals on kinematics needed for precise online myoelectric control?" *IEEE Transactions on Neural Systems and Rehabilitation Engineering*, vol. 22, no. 3, pp. 549–558, 2014.

[24] S. B. Godfrey, A. Ajoudani, M. G. Catalano, G. Grioli, and A. Bicchi, "A synergy-driven approach to a myoelectric hand," in *13TH International Conference on Rehabilitation Robotics*, June 24-26, 2013, Seattle, WA., 2013, pp. 1 – 6. [Online]. Available: 10.1109/ICORR.2013.6650377

[25] X. Liu, K. M. Mosier, F. A. Mussa-Ivaldi, M. Casadio, and R. A. Scheidt, "Reorganization of finger coordination patterns during adaptation to rotation and scaling of a newly learned sensorimotor transformation," *Journal of neurophysiology*, vol. 105, no. 1, pp. 454–473, 2011.

[26] D. J. Berger, R. Gentner, T. Edmunds, D. K. Pai, and A. d'Avella, "Differences in adaptation rates after virtual surgeries provide direct evidence for modularity," *The Journal of Neuroscience*, vol. 33, no. 30, pp. 12 384–12 394, 2013.

[27] M. Bonilla, E. Farnioli, C. Piazza, M. Catalano, G. Grioli, M. Garabini, M. Gabiccini, and A. Bicchi, "Grasping with soft hands," in *Humanoid Robots (Humanoids), 2014 14th IEEE-RAS International Conference on*. IEEE, 2014, pp. 581–587.

[28] N. Jiang, H. Rehbaum, I. Vujaklija, B. Graimann, and D. Farina, "Intuitive, online, simultaneous, and proportional myoelectric control over two degrees-of-freedom in upper limb amputees," *IEEE transactions on neural systems and rehabilitation engineering*, vol. 22, no. 3, pp. 501–510, 2014.

[29] J. M. Hahne, S. Dähne, H.-J. Hwang, K.-R. Müller, and L. C. Parra, "Concurrent adaptation of human and machine improves simultaneous and proportional myoelectric control," *IEEE Transactions on Neural Systems and Rehabilitation Engineering*, vol. 23, no. 4, pp. 618–627, 2015.

[30] A video of the activities performed with the softhand 2. [Online]. Available: https://www.dropbox.com/s/3q5nynsdgipjm57/Sim_and_prop_control.mp4?dl=0